Mainz Microtron MAMI

Collaboration A1: "Virtual Photons"

Spokesperson: H. Merkel

Proposal for an Experiment

Study of the Roper resonance in the $p(\vec{e}, e'\vec{p})\pi^0$ process

Collaborators:

P. Achenbach, C. Ayerbe Gayoso, J. C. Bernauer, R. Böhm, A. Denig,
M. O. Distler, A. Esser, M. Gómez, K. Grießinger, F. E. Maas, H. Merkel*, U. Müller,
L. Nungesser, J. Pochodzalla, T. Saito, S. Sánchez Majos, B. S. Schlimme,
M. Weinriefer
(Institut für Kernphysik, Universität Mainz)

H. Fonvieille
(LPC IN2P3-CNRS, Université Blaise Pascal, Clermont-Ferrand, France)

L. Debenjak, M. Potokar, S. Širca*
(University of Ljubljana and Institut "Jožef Stefan" Ljubljana, Slovenia)

D. Bosnar, I. Friščić, M. Makek
(Department of Physics, University of Zagreb, Croatia)

*Contact Person (E-Mail: simon.sirca@fmf.uni-lj.si, merkel@kph.uni-mainz.de)

Abstract

We propose to study the structure of the Roper resonance by a measurement of recoil proton polarization components in the $p(\vec{e}, e'\vec{p})\pi^0$ reaction. The components exhibit strong sensitivities to the resonant Roper multipoles M_{1-} and S_{1-}. These measurements will offer a unique insight for extracting information on the $N \rightarrow R$ transition through comparison with the state-of-the-art models, and will also provide severe constraints on these models in the second resonance region.

1   Introduction

The $P_{11}(1440)$ (Roper) resonance [1] is the lowest positive-parity $N^\star$ state. It is visible in partial-wave decompositions of $\pi N \to \pi N$ and $\pi N \to \pi\pi N$ scattering [2, 3] as a shoulder around $1440\,\mathrm{MeV}$ with a width of about $350\,\mathrm{MeV}$ [4]. Its large width causes it to merge with the adjacent $D_{13}(1520)$ and $S_{11}(1535)$ resonances, and therefore it can not be resolved from the W-dependence of the cross-section alone. Although this four-star resonance is within the energy range of many modern facilities, the experimental analyses so far have not ventured far beyond the determination of its mass, widths, and photon decay amplitudes. Very little is known about its internal structure.

The purpose of this experiment is to study the structure of the Roper resonance by measuring the recoil proton polarization components P'_x, P_y, and P'_z in the $p(\vec{e}, e'\vec{p})\pi^0$ reaction at a specific value of Q^2, W and centre-of-mass angle θ. In particular, the P'_z and P_y exhibit strong sensitivities to the resonant multipoles M_{1-} and S_{1-} relevant to Roper electro-production. Our measurements will provide vital input the state-of-the-art models of pion electro-production in the second resonance region. It is for the first time that the Roper resonance is being approached by means of the recoil-polarization technique, although this strategy benefits substantially from the experience gained in the well-studied $N \to \Delta$ transition.
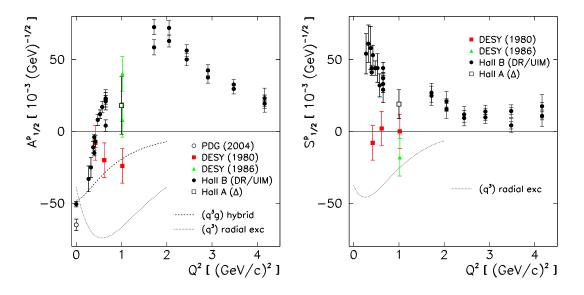
2   Physics overview and motivation

At present, only two models exist that are capable of computing full electro-production matrix elements with complex multipole structures. These models, and their connection to our measurement will be discussed in more detail in Subsection 2.2. On the other hand, numerous models have been developed to investigate the structure of the Roper resonance by studying the photo- and electro-excitation part of the process. These developments are summarized below.

In the simplest spherically symmetric quark model with SU(6) spin-flavour symmetry, the Roper resonance can be understood as a radial excitation of the proton, with one quark occupying the 2s state, yielding a $(1s)^2(2s)^1$ configuration. The spin, isospin and parity are assumed not to change in this transition, and hence the excitation can be viewed as a "breathing mode" of the proton. This physical picture implies a sizable Coulomb monopole contribution (C0 or S_{1-}) along with the only other allowed multipole, the magnetic dipole (M1 or M_{1-}).

Recent models [5, 6] have indicated a possible description of the Roper resonance as a gluonic partner of the proton, represented as a (q^3g) hybrid baryon. Hybrid baryons are states presumably dominated by the state of three quarks oscillating against explicitly excited configurations of the gluon fields. The energies of these excitations could be as low as $550\,\mathrm{MeV}$, so the Roper state is a natural candidate. The problem is that the hybrid states may have the same quantum numbers as the three-quark states, thus by spectroscopy alone, they are indistinguishable. However, hybrid and three-quark representations can be discriminated by virtue of different structures of the spatial and spin-flavour wave-functions. In hybrids, the radial

wave-functions of the proton and the Roper are the same, while the spin-isospin parts are orthogonal. Since the radial wave-functions are equal, the matrix element of the charge operator vanishes (to lowest relativistic order). The C0 strength should thus be highly suppressed, implying a predominantly magnetic dipole transition, in contrast to the concept of "breathing".

These two opposing concepts result in rather different predictions for the Q^2-dependence of the transverse ($A^p_{1/2}$) and scalar ($S^p_{1/2}$) electro-production helicity amplitudes shown in Fig. 1. In the charged channel, the radially excited (q^3) state is predicted to have a characteristically slow fall-off of $A^p_{1/2}$ and $S^p_{1/2}$ which seems to be excluded by the scarce data. The predicted Q^2-dependence of $A^p_{1/2}$ for the hybrid (q^3g) state has a fall-off similar to the one seen in the $N \to \Delta$ transition, while $S^p_{1/2}$ is predicted to be zero. The experimental photo-production data in the figure is from the PDG review [4], and both approaches mentioned above fail to reproduce these electromagnetic couplings.

Fig. 1 — Nucleon-Roper transverse (left) and scalar (right) helicity amplitudes for the charged (proton) state. Published experimental data are from [4] for the photon point and from analyses [7, 8] of old unpolarized electro-production data for $Q^2 > 0$. The preliminary CLAS and Hall A data are discussed in Section 2.1. The curves are for a Roper as a radially excited (q^3) state or a (q^3g) hybrid state [6].

Experimentally, the Q^2-dependence of the helicity amplitudes has become better known only recently. A re-analysis of old DESY and NINA electro-production experiments yielded $S^p_{1/2}$ consistent with zero, and gave contradictory results for the $A^p_{1/2}$. The lack of (double)-polarized measurements is, to a great extent, responsible for such large uncertainties. New experiments in Hall B at JLab have yielded a much better picture for the $S^p_{1/2}$ amplitude in a broad range of Q^2, and in particular for the $A^p_{1/2}$ amplitude, which now clearly exhibits a zero-crossing in the vicinity of $Q^2 \approx 0.5\,(\text{GeV/c})^2$.

The Roper has also been investigated as a hybrid baryon by using QCD sum rules [9] and in perturbative QCD [10]. The latter prediction states that if Roper is a hybrid, its electro-production rate should remain small asymptotically, whereas if it is a (q^3) state, it should not. In the most modern hybrid approaches [11, 12, 13], the Roper

masses are well understood in terms of vibrating flux-tubes between quarks, but extensions of the models to dynamical processes are still lacking. Perhaps, Lattice QCD is the tool which will help remove the numerous controversies surrounding the Roper. It has recently been observed clearly and at the correct energy on the lattice in a very precise calculation with a pion mass as low as 180 MeV [14]. This has been achieved in a quenched approximation, leading to a conclusion that the Roper resonance is a (q^3) state. Other identifications of the resonance have been reported [15, 16], but dynamical processes involving the Roper remain future work.

Extensive studies of the nature of the Roper resonance in constituent, non-relativistic, and relativized quark models also exist. In [17], the Roper has been studied in a semi-relativistic constituent-quark model with a linear confinement potential, resulting in a good description of the Roper mass and width, but it failed to reproduce the photo-couplings. A closer agreement has been achieved in a potential quark model where the relativistic electro-magnetic interaction Hamiltonian has been treated consistently to $\mathcal{O}(v^2/c^2)$ for the quarks [18]. This approach suggests that QCD configuration-mixing effects may have an increasingly large influence on helicity amplitudes with increasing Q^2. A further improvement has been advanced by [19, 20], in a quark model with relativistic corrections to the transition operator. However, the photo-couplings for the Roper resonance remained in disagreement with the data by roughly a factor of two. More recent quark-model calculations formulated on the light-front [21, 22, 23] have not improved this discrepancy significantly. In a non-relativistic quark model based on an extension of the Roper photo-production to $Q^2 > 0$ and by using vector-meson exchanges [24], a good agreement with the experimental couplings has been obtained.

The photo- and electro-excitation of the Roper resonance has also been approached in quark models with meson degrees of freedom. A fair understanding of the photo-couplings has been obtained if meson-exchange currents between quarks were introduced [25], as well as if the Roper is treated in a relativistic quark model as a three-quark core with an admixture of pions [26]. In the chiral chromo-dielectric model [27] (see also [28]), the Roper is described in terms of three valence quarks coupled to a cloud of chiral mesons (σ and π) and to a chromo-dielectric field which dynamically confines the quarks. The quarks are in the $(1s)^3$ configuration for the bare nucleon and $(1s)^2(2s)^1$ for the bare Roper, and the physical Roper emerges from a self-consistent variation of the radial fields. One of the outstanding features of this model is a strong meson cloud which has gained in merit in recent studies of the $N \rightarrow \Delta$ transition.

The importance of the pion cloud is inherent also to all versions of the cloudy bag model (CBM). Photo-couplings for the Roper resonance in the CBM have been calculated [29] and were found to depend strongly on the strength of the pion cloud. The analysis of [30, 31] also used CBM input to study the πN-scattering phase-shifts in the Roper region by examining the resonance widths with and without inclusion of the Roper as a radial excitation (a bare three-quark state). The results seem to exclude such a state.

2.1 Relation to other experiments

The region of the Roper resonance has been explored to various extents both at Jefferson Lab and MAMI. In most of the cases, only cross-sections (angular distributions) were measured. Only a handful of single- and double-polarization measurements have been performed so far.

Jefferson Lab: Hall B (CLAS)

Kinematically most extensive data sets on single-pion electro-production in the nucleon resonance regions come from Hall B. Angular distributions and W-dependence of the electron beam asymmetry $\sigma_{LT'}$ have been measured for both charged and neutral channels in the $P_{33}(1232)$ region at $Q^2 = 0.4$ and $0.65\,(\mathrm{GeV/c})^2$ [32, 33]. Very recently, dispersion-relation (DR) techniques and unitary isobar models (UIM) have been applied to analyze the CLAS $\sigma_{LT'}$ data in a much larger range of Q^2 and spanning also the second resonance region, in order to extract the contributions of the $P_{33}(1232)$, $P_{11}(1440)$, $D_{13}(1520)$, and $S_{11}(1535)$ resonances to single-pion production [34].

A complete angular coverage was achieved, and several relevant amplitudes could be separated in a partial-wave analysis restricted to $l \leq 2$. The Legendre moments D_0, D_1, and D_2 of the expansions

$$\sigma_\alpha = D_0 + D_1\,P_1(\cos\theta_\pi^\star) + D_2\,P_2(\cos\theta_\pi^\star) + \cdots$$

for different partial cross-sections σ_α (or corresponding structure functions) were determined: an example for $\sigma_\alpha \equiv \sigma_\mathrm{T} + \varepsilon\sigma_\mathrm{L}$ is furnished by Fig. 2. To achieve a good fit of θ_π^*- and W-dependence of $\sigma_{LT'}$, a simultaneous adjustment of the M_{1-} and S_{1-} amplitudes was needed. Since both the pπ^0 and the nπ^+ channel were measured (isospin), the transverse helicity amplitude $A_{1/2}^\mathrm{p} \propto_\mathrm{p} M_{1-}^{1/2}$ as well as the scalar $S_{1/2}^\mathrm{p} \propto_\mathrm{p} S_{1-}^{1/2}$ could be extracted. The results show a rapid fall-off of $A_{1/2}^\mathrm{p}$ and indicate its zero-crossing at $Q^2 \approx 0.5\,(\mathrm{GeV/c})^2$ (see Fig. 1).
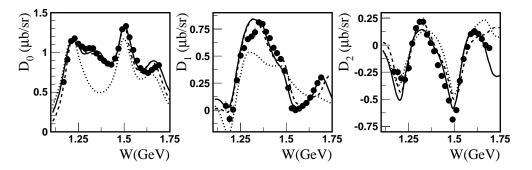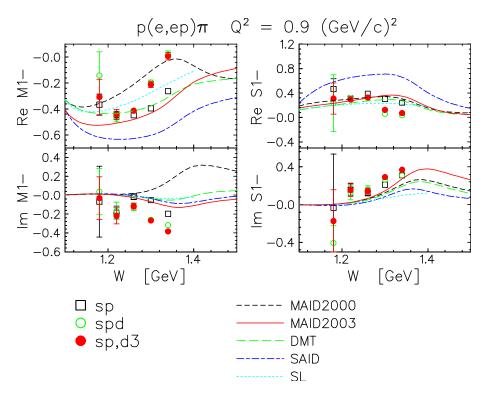

Fig. 2 — The lowest Legendre moments of the $\sigma_\mathrm{T} + \varepsilon\sigma_\mathrm{L}$ structure function for charged pion electroproduction at $Q^2 = 2.05\,\mathrm{GeV}^2$. The solid and dashed curves correspond to the DR and UIM results, respectively. The dotted curves have been obtained by switching off the Roper resonance in the final results.

In Hall B, there is also an approved experiment E03-105 [36] to measure single-pion photo-production in both p(γ, π^+)n and p$(\gamma, \mathrm{p})\pi^0$ channels, with polarized beam and longitudinally and transversely polarized target using CLAS. It will measure

two single- (T and P) and three double-polarization observables (G, F, and H); in addition, the experiment E01-104 will measure the double-polarization observable E. The measurements will span the range $1300 \leq W \leq 2150\,\mathrm{MeV}$ and achieve an angular coverage of $-0.9 \leq \cos\theta^\star \leq 0.9$. Due to the forthcoming energy upgrade of CEBAF, it remains unclear whether any of these experiments will run in the nearby future.

It is believed that this data will greatly constrain partial-wave analyses in photo-production and reduce model-dependent uncertainties in the extraction of nucleon resonance properties. A similar goal, but in electro-production, and utilizing the recoil-polarimetry technique, has been put forward by the Hall A Collaboration at JLab [37]. To some extent this experiment would be complementary to the effort with CLAS. However, due to Laboratory beam-time constraints, it has been deferred.
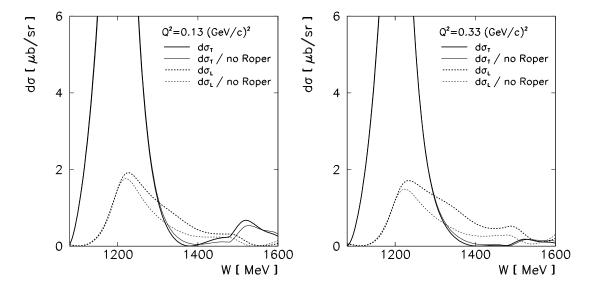
Jefferson Lab: Hall A

Polarized electron beam and recoil-polarimetry capability of Hall A also allow access to double-polarization observables in single-pion electro-production. Recoil-polarization observables are composed of different combinations of multipole amplitudes than observables accessible in the case of a polarized target.

Fig. 3 — The W-dependence of the Re and Im parts of M_{1-} and S_{1-} multipoles in the $\mathrm{p}(\vec{e}, e'\vec{p})\pi^0$ channel (results of the Hall A E91-011 experiment [39]).

The acceptance of CLAS is large enough to achieve a complete angular coverage of the outgoing hadrons. This is not possible in the case of relatively small angular openings of the Hall A HRS spectrometers *except* at high Q^2 where the Lorentz boost from the center-of-mass to lab frame focuses the reaction products into a cone narrow enough to provide a virtually complete out-of-plane acceptance. The

E91-011 experiment in Hall A in the $p(\vec{e}, e'\vec{p})\pi^0$ channel [38] was performed at sufficiently high $Q^2 = (1.0 \pm 0.2)\,(\mathrm{GeV/c})^2$ and $W = (1.23 \pm 0.02)\,\mathrm{GeV}$ to allow for a measurement of all accessible response functions, even those that vanish for coplanar kinematics. Two Rosenbluth combinations and 14 structure functions could be separated, allowing for a restricted partial-wave analysis giving access to all $l \leq 1$ multipole amplitudes relevant to the $N \to \Delta$ transition. The results for the M_{1-} and S_{1-} multipoles in the $p\pi^0$ channel are shown in Fig. 3. Both multipoles indicate a rising trend approaching the $W \sim 1440\,\mathrm{MeV}$ region, again pointing towards the Roper.

Unfortunately, the cross-sections at $W \sim 1440\,\mathrm{MeV}$ (for any Q^2) are about an order of magnitude smaller than in the Δ-peak (see Fig. 4). For high $Q^2 \sim 1\,(\mathrm{GeV/c})^2$, where a large out-of-plane coverage would allow for a decent partial-wave analysis in Hall A, the cross-sections are even smaller. Furthermore, due to the zero-crossing uncertainty of the M_{1-} multipole, it is not clear what value of Q^2 to choose in order to have a prominent $M1$ signal. Furthermore, models indicate that the crucial features of the Roper multipoles (or helicity amplitudes) are visible at relatively small Q^2 of a few $0.1\,(\mathrm{GeV/c})^2$, nullifying the boost-advantage of the HRS spectrometers.

Fig. 4 — The W-dependence of the transverse and longitudinal CM cross-sections at $Q^2 = 0.1$ and $0.3\,(\mathrm{GeV/c})^2$, with the contribution of the Roper resonance on and off (MAID calculation).

We note in addition that higher partial waves ($l \geq 2$) in all JLab partial-wave analyses so far needed to be constrained by models (just as in the CLAS experiments). Thus, even with (almost) complete angular coverages, existing data sets of finite statistical certainty do not allow for a "full" partial-wave analysis to sufficiently large l.

MAMI: A2

In photo-production, the double-polarization asymmetry G for linearly polarized photons (P_γ) and target nucleons polarized longitudinally (P_z) along the photon momentum, exhibits a very strong sensitivity to the Roper resonance. It is defined

as
$$G = \frac{d\sigma(\Phi = 45°, z) - d\sigma(\Phi = -45°, z)}{d\sigma(\Phi = 45°, z) + d\sigma(\Phi = -45°, z)} \, ,$$
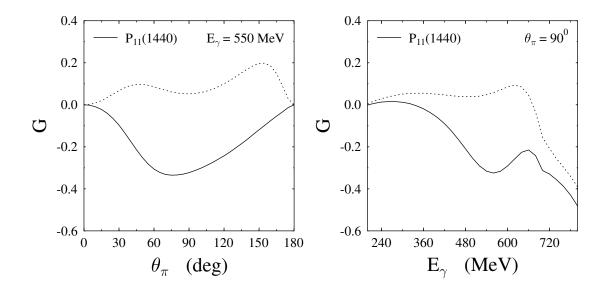
where Φ is the angle between the photon polarization plane and the reaction plane. The cross-section has the form

$$d\sigma(\theta_\pi, \Phi) = d\sigma(\theta_\pi)\Big(1 - P_\gamma \Sigma(\theta_\pi) \cos 2\Phi + P_\gamma P_z \, G(\theta_\pi) \sin 2\Phi \Big) \, .$$

In the $\vec{\gamma}\vec{p} \to p\pi^0$ reaction, G depends on the interference of the much better-known M_{1+} multipole governed by the $\Delta(1232)$, and the M_{1-} driven by the Roper,

$$G(\theta_\pi) \simeq \sin^2 \theta_\pi \, \text{Im}M_{1+} \, \text{Re}M_{1-} \, .$$

The asymmetry G will be measured by virtue of its $\sin 2\Phi$-dependence at the A2 Collaboration at MAMI with the Φ-symmetric detector DAPHNE. The expected sensitivity is shown in Fig. 5. In addition to the $p\pi^0$, the $n\pi^+$ channel will be measured, allowing for the isospin decomposition of the partial waves.
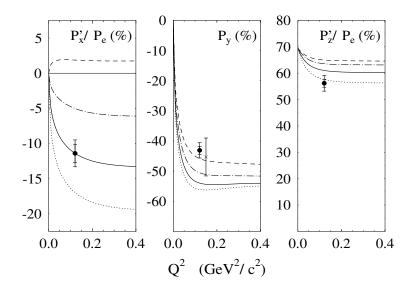

Fig. 5 — MAID prediction for G in $\vec{\gamma}\vec{p} \to p\pi^0$: angular distribution at $W = 1440\,\text{MeV}$ and energy dependence at $\theta_\pi = 90°$. The dotted curves correspond to the Roper switched off.

MAMI: A1

All three recoil polarization components (P'_x/P_e, P_y, and P'_z/P_e) in the $p(\vec{e}, e'\vec{p})\pi^0$ reaction at the Δ resonance, at $Q^2 = 0.121\,(\text{GeV/c})^2$ have been measured by the A1 Collaboration at MAMI [40] (see Fig. 6).

These components, in particular the P'_x, were shown to be highly sensitive to the Coulomb quadrupole to magnetic dipole ratio CMR $= \text{Im}S_{1+}^{(3/2)}/\text{Im}M_{1+}^{(3/2)}$ in the $N \to \Delta$ transition. Note, however, that the changes in the CMR (i.e. in the corresponding S_{1+} multipole) between the curves in Fig. 6 are quite large ($\pm 50\,\%$).

Note that a straight-forward extension of the $N \to \Delta$ program in the $\vec{p}\pi^0$ channel into the Roper region appears to be impossible at Mainz/A1 due to instrumental constraints.

Fig. 6 — MAMI results for the recoil polarization components in $p(\vec{e}, e'\vec{p})\pi^0$ at $W = 1232 \, \text{MeV}$ and $Q^2 = 0.121 \, (\text{GeV/c})^2$, compared to MAID 2000 calculations. The dashed, dot-dashed, full, and dotted curves correspond to CMR $= \text{Im} S_{1+}^{(3/2)}/\text{Im} M_{1+}^{(3/2)}$ of $0\,\%$, $-3.2\,\%$, $-6.4\,\%$, and $-9.6\,\%$, respectively.

2.2 Relevance to pion electro-production models

The numerous models mentioned in the Introduction, although conceptually rich, are not in a stage at which they could be confronted with double-polarization observables with complex multipole structures, mostly because of an incomplete treatment of backgrounds, or due to an inability to include higher resonances. For a comprehensive description of resonance dynamics, three state-of-the-art pion electro-production models are available: the unitary isobar model MAID [41] and the dynamical models of the Dubna-Mainz-Taipei group (DMT) [42, 43] and Sato and Lee (SL) [44]. All these models were put to thorough verification when exposed to recent $N \to \Delta$ transition double-polarization data from MIT-Bates, MAMI, and JLab, with varying success. Extrapolations into the Roper region remain a challenge for all, and two of them (MAID and DMT) can be directly tested with our proposed measurements.

Unitary isobar model (MAID)

The **MAID** model is based on effective Lagrangians with numerous adjustable parameters. The backgrounds are described by nucleon Born terms and vector-meson exchange terms, while the resonant contributions to each of the electro-production multipoles are parameterized by Breit-Wigner forms. The total amplitude is unitarized.

In MAID, the imaginary parts of the M_{1-} and S_{1-} multipoles for isospin 1/2 are dominated by the resonant contributions. Therefore, the separation of the resonance from the background is relatively unproblematic for the Roper, the main challenge is a good determination of the multipoles themselves. A partial-wave analysis is therefore essential, and it can only be improved by measuring very sensitive observables that are used in the fits. In photo-production, high-quality data are available, and the multipole analyses over extended W-ranges result in good global fits.

In electro-production, additional precise measurements of both cross-sections and (double-)polarization observables are badly needed in order to stabilize the fits.

Ideally, partial-wave analyses require complete data sets taken at particular values of Q^2. In reality, for example, CLAS has acquired "low-Q^2" data while Hall A covered a narrow range at "high Q^2". The MAID group therefore has recently been pursuing another direction by proposing "super-global" partial-wave analyses in which the Q^2-dependence of the multipoles is also parameterized by smooth functions. Such an analysis is then "fed" by practically all available photo- and electro-production data.

This approach is expected to work, and can even be refined, for smaller ranges in Q^2 and W. Following this guideline [48], we shall restrict the Q^2-coverage to the range $0 < Q^2 < 1\,(\mathrm{GeV/c})^2$, and span a controllable energy range ($\simeq 100\,\mathrm{MeV}$) in the vicinity of the resonance position. We depart intentionally, and with a purpose, from the well-established practice of measuring (only) at the resonance position: the energy dependence is badly needed for robust fits.

Dynamical models (DMT, SL)

The crucial feature of the dynamical (microscopic) approaches to pion electro-production is the inclusion of the final-state πN interaction such that the unitarity is preserved in the theory. In the **DMT model**, this is achieved by coupling the $\gamma^\star N \to \pi N$ transition potential to the πN t-matrix, where the transition potential consists of the background part and the bare resonance part.

In the following, we use the most recent version of the DMT model (2001) and the MAID model (2003) in comparisons.
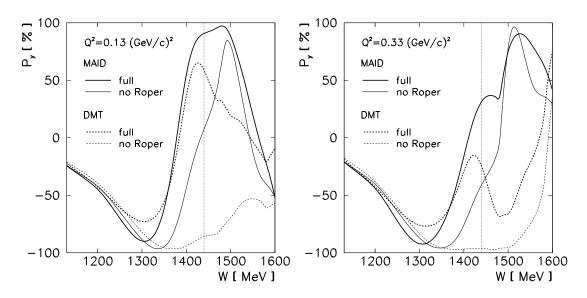

Fig. 7 — The MAID and DMT predictions for the W-dependence of P_n at $Q^2 = 0.13$ and $0.33\,(\mathrm{GeV/c})^2$, with the contribution of the Roper resonance on and off.

While MAID and DMT agree on the cross-sections, they predict quite different Q^2- and W-dependences of recoil polarization amplitudes (in particular the P_y), and exhibit distinct sensitivities to the Roper multipoles (see Fig. 7). The variation in the

9

sensitivities is due to the difference in the way resonances are treated in isobar models like MAID, compared to that in dynamical models like DMT. In isobar models, the EM vertices of resonances are "dressed" (i.e. they already contain pion-cloud contributions), so the resonance parameters in these models are directly comparable to the experimentally determined (PDG) values. In dynamical models, the resonances are "bare", and thus more consistent with e.g. quark-model predictions. The proposed measurement will be an important step towards drawing a distinction between the "dressed" and "bare" approaches.

At present, the **SL model** is not applicable to the meson electro-production reactions above the delta resonance region. Attempts are being made to extend the model to higher energies, but the extension requires considerable effort. The authors do believe [47] that it is important to map the energy- and Q^2-dependence of the P_{11} amplitudes in constraining the nature of Roper resonance and dynamics in the 1.4 GeV region.

3 Formalism of the $p(\vec{e}, e'\vec{p})\pi^0$ reaction

The cross-section for the $p(\vec{e}, e'\vec{p})\pi^0$, allowing for both a polarized electron beam and detection of the recoil proton polarization, is given by [49]

$$\frac{d\sigma}{dE_e' \, d\Omega_e \, d\Omega_p^\star} = \frac{\sigma_0}{2} \left\{ 1 + \boldsymbol{P} \cdot \widehat{\boldsymbol{s}}_r + h \left[A_e + \boldsymbol{P}' \cdot \widehat{\boldsymbol{s}}_r \right] \right\}, \tag{1}$$

where $\sigma_0 \equiv d\sigma(\widehat{\boldsymbol{s}}_r) + d\sigma(-\widehat{\boldsymbol{s}}_r)$ is the unpolarized cross-section, $\widehat{\boldsymbol{s}}_r$ is the proton spin vector in its rest frame, h is the helicity of the incident electrons, $\boldsymbol{P}$ is the induced proton polarization, A_e is the beam analyzing power, and $\boldsymbol{P}'$ is the vector of spin-transfer coefficients. The polarization of the recoiled proton consists of a helicity-independent (induced) and a helicity-dependent (transferred) part, $\boldsymbol{\Pi} \equiv \boldsymbol{P} + h\boldsymbol{P}'$. The cross-section can be cast in a form in which the electron vertex is evaluated in the lab frame, while hadronic quantities are in the CM frame of the πN final state. In terms of response functions, the cross-section is

$$\begin{aligned}
\frac{d\sigma}{dE_e' \, d\Omega_e \, d\Omega_p^\star} = \Gamma_v \frac{|\boldsymbol{p}_p^\star| W}{K_\gamma M_p} \Big\{ & (R_T + R_T^n S_n) + 2\varepsilon_L^\star (R_L + R_L^n S_n) \\
& + \sqrt{\varepsilon_L^\star(1+\varepsilon)} \Big[(R_{LT} + R_{LT}^n S_n) \cos\phi + (R_{LT}^l S_l + R_{LT}^t S_t) \sin\phi \Big] \\
& + \varepsilon \Big[(R_{TT} + R_{TT}^n S_n) \cos 2\phi + (R_{TT}^l S_l + R_{TT}^t S_t) \sin 2\phi \Big] \\
& + h\sqrt{\varepsilon_L^\star(1-\varepsilon)} \Big[(R_{LT}' + R_{LT}'^n S_n) \sin\phi + (R_{LT}'^l S_l + R_{LT}'^t S_t) \cos\phi \Big] \\
& + h\sqrt{1-\varepsilon^2} \Big[R_{TT}'^l S_l + R_{TT}'^t S_t \Big] \Big\},
\end{aligned} \tag{2}$$

where M_p is the proton mass, W is the invariant mass of the πN final state, Γ_v is the virtual photon flux, and $K_\gamma = (W^2 - M_p^2)/2W$ is the equivalent real-photon energy. The ε is the transverse polarization of the virtual photon.

The subscripts T, L, LT, and TT denote transverse, longitudinal, longitudinal-transverse, and transverse-transverse interference terms, the primes denote those response functions which can only be accessed by using polarized electrons, and

the * denotes CM quantities. The longitudinal polarization of the virtual photon is $\varepsilon_L^\star \equiv \varepsilon(Q^2/|\boldsymbol{q}^\star|^2)$, and $S_{n,l,t}$ are the projections of the proton spin vector, given by $S_t = \hat{\boldsymbol{t}} \cdot \hat{\boldsymbol{s}}_r$, $S_n = \hat{\boldsymbol{n}} \cdot \hat{\boldsymbol{s}}_r$, and $S_l = \hat{\boldsymbol{l}} \cdot \hat{\boldsymbol{s}}_r$. The projections are given in the coordinate frame of the reaction plane which is tilted at an angle of $\phi_{pq}^\star \equiv \phi$ with respect to the electron scattering plane (see Fig. 8), $\hat{\boldsymbol{l}}$ is along the proton momentum, $\hat{\boldsymbol{n}}$ is normal to the reaction plane, and $\hat{\boldsymbol{t}} = \hat{\boldsymbol{n}} \times \hat{\boldsymbol{l}}$.
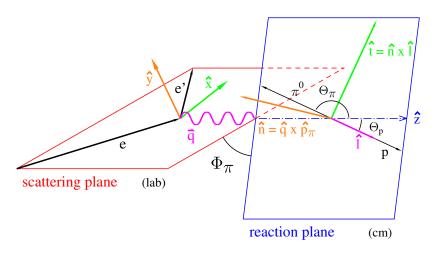

Fig. 8 — Schematic representation of the $\mathrm{p}(\vec{e}, e'\vec{p})\pi^0$ reaction.

For measurements in the (e, e') scattering plane, the polarization components $\boldsymbol{\Pi}$ can be extracted by comparing coefficients in (1) and (2) and by using $\boldsymbol{\Pi} \cdot \hat{\boldsymbol{s}}_r = \Pi_t S_t + \Pi_n S_n + \Pi_l S_l$,

$$\tilde{\sigma}_0 \Pi_t = h\left[\sqrt{1 - \varepsilon^2}\, R_{TT}'^t \pm \sqrt{\varepsilon_L^\star(1 - \varepsilon)}\, R_{LT}'^t \right],$$

$$\tilde{\sigma}_0 \Pi_n = R_T^n + 2\varepsilon_L^\star R_L^n \pm \sqrt{\varepsilon_L^\star(1 + \varepsilon)}\, R_{LT}^n + \varepsilon\, R_{TT}^n,$$

$$\tilde{\sigma}_0 \Pi_l = h\left[\sqrt{1 - \varepsilon^2}\, R_{TT}'^l \pm \sqrt{\varepsilon_L^\star(1 - \varepsilon)}\, R_{LT}'^l \right],$$

where $\tilde{\sigma}_0$ is the unpolarized cross-section, except for a term proportional to σ_{Mott},

$$\tilde{\sigma}_0 = R_T + 2\varepsilon_L^\star R_L \pm \sqrt{\varepsilon_L^\star(1 + \varepsilon)}\, R_{LT} + \varepsilon\, R_{TT},$$

and the $\pm$ signs correspond to $\phi = 0°$ and $180°$, respectively. The polarization components which are of interest to us have the following alternative notations: $P_x' \leftrightarrow -P_t$, $P_n \leftrightarrow P_y$, and $P_z' \leftrightarrow -P_l$.

In certain aspects, it would be favourable to go to parallel and antiparallel kinematics because some of the terms in the multipole expansion of the structure functions drop out, but the A1 spectrometer setup imposes severe restrictions on the type of kinematics that can be achieved (see below in section 4).

The structure functions contain the following combinations of the multipoles relevant for the Roper (the corresponding polarization component is given in the bracket before the structure function):

$$(P_n)R_T^n = -\mathrm{Im}\, E_{0+}^* (3E_{1+} + M_{1+} + 2M_{1-})$$

11

contains the leading M_{1-} amplitude in the imaginary part of the interference with the E_{0+} non-resonant amplitude; this is matched with the

$$(P_\mathrm{l})R^\mathrm{l}_\mathrm{TT'} \propto \mathrm{Re}\, E^*_{0+} \left(3E_{1+} + M_{1+} + 2M_{1-}\right)$$

response which contains the real part of the same interference. The terms

$$
\begin{aligned}
(P_\mathrm{n})R^\mathrm{n}_\mathrm{TL} \quad &\text{contains} \quad \mathrm{Im}\, L^*_{1-}M_{1-}\,, \\
(P_\mathrm{l})R^\mathrm{l}_\mathrm{TL'} \quad &\text{contains} \quad \mathrm{Re}\, L^*_{1-}M_{1-}
\end{aligned}
$$

contain nice (real and imaginary) interferences of both resonant multipoles but these are probably useless because both are very small. In addition, there are the

$$
\begin{aligned}
(P_\mathrm{n})R^\mathrm{n}_\mathrm{L} \quad &\propto \quad -2\,\mathrm{Im}\, L^*_{0+}\left(2L_{1+} - L_{1-}\right)\,, \\
(P_\mathrm{t})R^\mathrm{t}_\mathrm{TL'} \quad &\propto \quad \mathrm{Re}\left\{ L^*_{0+}\left(2M_{1+} + M_{1-}\right) + \left(2L^*_{1+} - L^*_{1-}\right) E_{0+} + \cdots \right\}
\end{aligned}
$$

terms, as well as the

$$(P_\mathrm{n})R^\mathrm{n}_\mathrm{TT} \quad \text{contains} \quad \sin\theta \cos\theta\, M^*_{1+}M_{1-}\,.$$

The latter term would be great to extract but as we show in the following, we shall be restricted to $\theta = 90°$ and thus this term will not be accessible.

4   Proposed measurement

Wishing to cover a reasonably broad kinematic range in the Roper region, one typically encounters angular and momentum settings and focal-plane polarimetry conditions which are unfavourable for the A1 spectrometer setup (assuming the existence of a fully equipped and operational KAOS spectrometer).

However, a good compromise can be found by going to non-parallel (or non-anti-parallel) kinematics for the proton. By doing this, we sacrifice some of the high sensitivities to the inclusion/exclusion of the Roper seen in the predicted polarization components, but we tune the kinematics such that we balance well between the physics sensitivities and maintaining good figures-of-merit for the FPP, as well as satisfying all geometry and momentum requirements. We propose the following baseline kinematics:

$E_\mathrm{e} = 1500\,\mathrm{MeV}$, $Q^2 = 0.1\,\mathrm{GeV}^2$, $W = 1440\,\mathrm{MeV}$, $\theta_\mathrm{cms} = 90°$

$E'_\mathrm{e} = 811\,\mathrm{MeV/c}$, $\theta_\mathrm{e} = 16.5°$ (Spec B)

$p_\mathrm{p} = 668\,\mathrm{MeV/c}$, $T_\mathrm{p} = 214\,\mathrm{MeV}$, $\theta_\mathrm{p} = 54.2°$ (Spec A)

The proton kinetic energy in the center of the carbon secondary scatterer in the FPP is about $T_\mathrm{cc} \approx 200\,\mathrm{MeV}$, which translates into a favourable figure-of-merit (FOM) of about $f_\mathrm{FPP} \approx 0.006$. The FOM drops to ≈ 0.003 for $\theta \approx 75°$.

The following estimates have been done with the dipole approximation for the precession matrix ($\chi \approx 215°$), assuming 100 h of 10 μA beam with $P_\mathrm{e} = 75\,\%$ polarization on a 5 cm LH$_2$ target, and reasonably conservative cuts in the simulation.
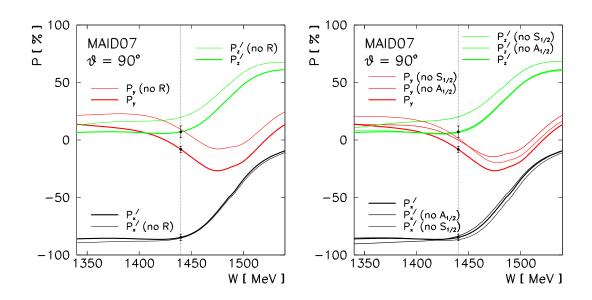
Fig. 9 — Expected uncertainties on P'_x, P_y and P'_z for 100 h beamtime; W-dependence.

One obtains ≈ 7000 counts/hour (before the FPP cuts) and the error estimates (for $\theta = 90°$)

$$\Delta P'_x = \frac{1}{P_e}\sqrt{\frac{2}{N_0\,f}} \approx 0.029$$

$$\Delta P_y = \frac{1}{\cos\chi}\sqrt{\frac{2}{N_0\,f}} \approx 0.027$$

$$\Delta P'_z = \frac{1}{P_e}\frac{1}{\sin\chi}\sqrt{\frac{2}{N_0\,f}} \approx 0.051$$

Figure 9 shows what can be achieved under these assumptions for the polarization components P'_x, P_y and P'_z, shown here as a function of W. One can see that we are sensitive mostly to transverse helicity amplitudes and that P'_x in some sense is useless except for calibration purposes.

Figure 10 shows the θ-dependence of the polarization components and what can be achieved under these assumptions in 200 h total beamtime. The expected error bars for $\theta = 90°$ and $\theta = 75°$ are shown. these are the two extreme angles that limit the angular range accessible with the current setup in relatively short beamtimes on the order of a week or two. Nothing above $\theta \approx 95°$ is doable at the moment because it exceeds the maximum p_p in Spec A. Also, nothing below $\theta \approx 75°$ is doable because the FPP FOM decreases too much at low p_p.

Even with two isolated points ($\theta = 90°$ and $\theta = 75°$), a strong physics case can be made. Figure 11 shows the sensitivities of the proposed measurement (100 h beamtime at each θ) to switching the Roper resonance contribution on and off in MAID2007 and DMT2001 models. These differences may highlight the effects of different treatments of resonances in isobar models (MAID) vs. those of dynamical models (DMT), that is, of having "dressed" vs. "bare" resonant vertices. From this perspective, one sees nice distinctions in all components of $\vec{P}$, and they can easily be probed with the proposed accuracy. Figure 12 shows the MAID-DMT comparison for full calculations only, as a function of W at $\theta = 90°$ (left), and as a function of θ at $W = 1440\,\mathrm{MeV}$ (right).
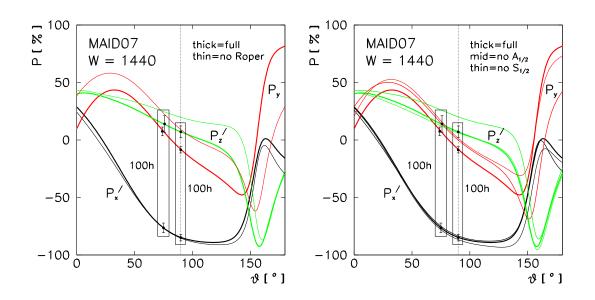
13

Fig. 10 — Expected uncertainties on P'_x, P_y and P'_z for 100 h beamtime; θ-dependence. The error bars in the figure are achievable with 200 h total beamtime (about half of that time for $\theta = 90°$ and half for $\theta = 75°$).

5   The focal-plane polarimeter

The A1 FPP is presently built into Spec A and has the efficiency shown in Figure 13 (private communication by H. Fonvieille and P. Janssens). The figure-of-merit is the integrated efficiency defined as

$$\text{FOM} \equiv f = \int_{\theta_{\min}}^{\theta_{\max}} \varepsilon(\theta) A_y^2(\theta) \mathrm{d}\theta \,,$$

where usually $\theta_{\min} = 7°$ and $\theta_{\max} = 20°$ are taken.

6   Count-rate estimates and beam-time request

For the $\theta = 90°$ kinematics, $p_{\mathrm{p}} = 668\,\text{MeV/c}$, $T_{\mathrm{p}} = 214\,\text{MeV}$, and taking proton energy loss in carbon into account, $T_{\mathrm{cc}} \approx 200\,\text{MeV}$, which corresponds to FOM $\approx$ 0.006. For 100 h beamtime, this implies the errors on the polarizations $\Delta P'_x \approx 0.029$, $\Delta P_y \approx 0.027$, and $\Delta P'_z \approx 0.051$. Note this is without taking into account the error propagation when reconstructing the target polarization values from the focal-plane polarizations.

For the $\theta = 75°$ kinematics, $p_{\mathrm{p}} = 569\,\text{MeV/c}$, $T_{\mathrm{p}} = 159\,\text{MeV}$, and taking proton energy loss in carbon into account, $T_{\mathrm{cc}} \approx 150\,\text{MeV}$, which corresponds to FOM $\approx$ 0.0035. For 100 h beamtime, this implies the errors on the polarizations $\Delta P'_x \approx$ 0.041, $\Delta P_y \approx 0.038$, and $\Delta P'_z \approx 0.072$.

We request 14 days of beamtime with 1.5 GeV CW beam. We require 10 μA beam with 75 % polarization and the standard 5 cm cryogenic LH$_2$ target. The beamtime request consists of 200 h ideal pure production running assuming $\approx$ 3/4 efficiency and 72 hours for calibration purposes.
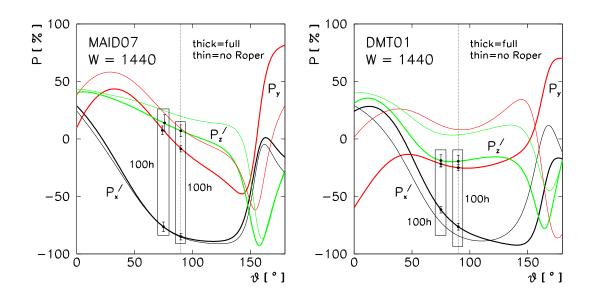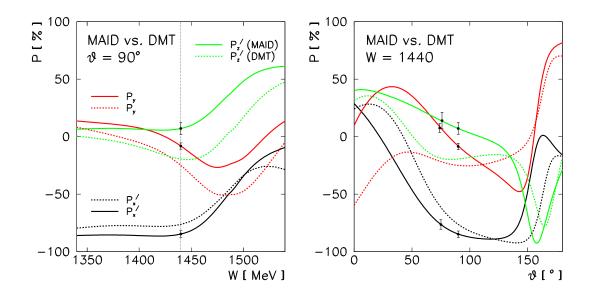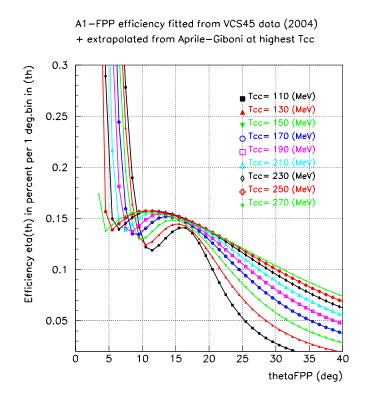
Fig. 11 — Recoil polarization components P'_x, P_y and P'_z as functions of θ in MAID2007 and DMT2001, with Roper on and off. The anticipated uncertainties for 100 h beamtime at each θ are shown. Everything is at $Q^2 = 0.1\,\mathrm{GeV}^2$.

Fig. 12 — Full calculations of MAID and DMT models for P'_x, P_y and P'_z as a function of W at $\theta = 90°$ (left), and as a function of θ at $W = 1440\,\mathrm{MeV}$ (right).

15

Fig. 13 — Efficiency of the A1 FPP. The $T_{\rm cc} = 110\,{\rm MeV}$ curve corresponds to $p_{\rm p} = 470\,{\rm MeV/c}$ and the $T_{\rm cc} = 270\,{\rm MeV}$ to $p_{\rm p} = 760\,{\rm MeV/c}$. These are the extreme values at which this FPP can be operated. The $\theta = 90°$ kinematics requires $p_{\rm p} = 668\,{\rm MeV/c}$ ($T_{\rm cc} \approx 200\,{\rm MeV}$), while the $\theta = 75°$ kinematics requires $p_{\rm p} = 569\,{\rm MeV/c}$ ($T_{\rm cc} \approx 150\,{\rm MeV}$).

6.1 Further options (involving KAOS)

The kinematics coverage of the proposed experiment could be significantly improved, and the physics case strongly enhanced, if a focal-plane polarimeter would be available for the newly installed KAOS spectrometer. One would be able to go to parallel or anti-parallel kinematics for the proton and thereby probe the regions in W and θ where the recoil polarization components are much more sensitive to the Roper resonance. In fact, such a hardware upgrade is foreseen in the nearby future.

References

[1] L. D. Roper, Phys. Rev. Lett. **12** (1964) 340.

[2] D. M. Manley, E. M. Saleski, Phys. Rev. D **45** (1992) 4002.

[3] R. E. Cutkosky, C. P. Forsyth, R. E. Hendrick, R. L. Kelly, Phys. Rev. D **20** (1979) 2839.

[4] S. Eidelman et al. (Particle Data Group), Phys. Lett. B **592** (2004) 1.

[5] Z. Li, Phys. Rev. D **44** (1991) 2841.

[6] Z. Li, V. Burkert, Z. Li, Phys. Rev. D **46** (1992) 70.

[7] C. Gerhardt, Z. Phys. C **4** (1980) 311.

[8] B. Boden, G. Krösen, Research Program at CEBAF, Report of the 1986 Summer Study Group, V. Burkert (ed.), p. 121.

[9] L. S. Kisslinger, Z. Li, Phys. Rev. D **51** (1995) R5986.

[10] C. E. Carlson, N. C. Mukhopadhyay, Phys. Rev. Lett. **67** (1991) 3745.

[11] S. Capstick, P. R. Page, Phys. Rev. D **60** (1999) 111501.

[12] G. L. Strobel, K. V. Shitikova, Phys. Rev. C **56** (1997) 551.

[13] G. L. Strobel, Int. J. Theor. Phys. **39** (2000) 115.

[14] N. Mathur et al., `arXiv:hep-ph/0306199`.

[15] Y. Chen et al., `arXiv:hep-ph/0306199`.

[16] D. Guadagnoli, M. Papinutto, S. Simula, `arXiv:hep-lat/0409011`.

[17] Fl. Stancu, P. Stassart, Phys. Rev. D **41** (1990) 916.

[18] Z. Li, F. E. Close, Phys. Rev. D **42** (1990) 2207.

[19] S. Capstick, Phys. Rev. D **46** (1992) 1965.

[20] S. Capstick, Phys. Rev. D **46** (1992) 2864.

[21] H. J. Weber, Phys. Rev. C **41** (1990) 2783.

[22] S. Capstick, B. D. Keister, Phys. Rev. D **51** (1995) 3598.

[23] F. Cardarelli, E. Pace, G. Salmè, S. Simula, Phys. Lett. B **397** (1997) 13.

[24] F. Cano, P. González, Phys. Lett. B **431** (1998) 270.

[25] U. Meyer, A. J. Buchmann, A. Faessler, Phys. Lett. B **408** (1997) 19.

[26] Y. B. Dong, K. Shimizu, A. Faessler, A. J. Buchmann, Phys. Rev. C **60** (1999) 035203.

[27] P. Alberto, M. Fiolhais, B. Golli, J. Marques, Phys. Lett. B **523** (2001) 273.

[28] Th. Meissner, F. Grümmer, K. Goeke, M. Harvey, Phys. Rev. D **39** (1989) 1903.

[29] K. Bermuth, D. Drechsel, L. Tiator, J. B. Seaborn, Phys. Rev. D **37** (1988) 89.

[30] B. C. Pearce, I. R. Afnan, Phys. Rev. C **40** (1989) 220.

[31] J. A. Elsey, I. R. Afnan, Phys. Rev. C **40** (1989) 2353.

[32] K. Joo et al. (CLAS Collaboration), Phys. Rev. C **68** (2003) 032201(R).

[33] K. Joo et al. (CLAS Collaboration), Phys. Rev. C **70** (2004) 042201(R).

[34] I. Aznauryan et al. (Hall B Collaboration), Phys. Rev. C **78** (2008) 045209.

[35] L. Tiator et al., Eur. Phys. J. A **19** (2004) 55.

[36] N. Benmouna, G. O'Rielly, I. Strakovski, S. Strauch, JLab Experiment E03-105.

[37] O. Gayou, S. Gilad, S. Širca, A. Sarty (co-spokespersons), JLab Proposal PR05-010.

[38] J. J. Kelly, A. Sarty, S. Frullani (co-spokespersons), JLab Experiment E91-011.

[39] J. J. Kelly et al. (Hall A Collaboration), Phys. Rev. Lett. **95** (2005) 102001; see also J. J. Kelly et al. (Hall A Collaboration), Phys. Rev. C **75** (2007) 025201.

[40] Th. Pospischil et al. (A1 Collaboration), Phys. Rev. Lett. **86** (2001) 2959.

[41] D. Drechsel, O. Hanstein, S.S. Kamalov, L. Tiator, Nucl. Phys. **A** 645 (1999) 145.

[42] S. S. Kamalov, S. N. Yang, Phys. Rev. Lett. **83** (1999) 4494.

[43] S. S. Kamalov et al., Phys. Rev. C **64** (2001) 032201(R).

[44] T. Sato, T.-S.H. Lee, Phys. Rev. C **63** (2001) 055201.

[45] `http://www.kph.uni-mainz.de/MAID/maid2003/maid2003.html`

[46] `http://www.kph.uni-mainz.de/MAID/dmt/dmt2001.html`

[47] T. Sato, private communication (2004).

[48] L. Tiator, contribution to NSTAR 2004 (in preparation), and private communication (2004).

[49] A. Picklesimer, J. W. van Orden, Phys. Rev. C **35** (1987) 266.

[50] L. Pentchev, J. J. LeRose, JLab-TN-01-052 (2001).

[51] S. Escoffier, PhD Thesis (2001); see also JLab-TN-01-052 (2001).

[52] J. Lightbody, J. S. O'Connell, Computers in Physics **2** (1988) 57.

[53] C. Hyde-Wright, A. Nathan (co-spokespersons), JLab Experiment E99-114.